Rosuvastatin- and Heparin-Loaded Poly(L-lactide-co-caprolactone) Nanofiber Aneurysm Stent Promotes Endothelialization via Vascular Endothelial Growth Factor Type A Modulation

Peixi Liu,[†,#] Yingjun Liu,[†,#] Peiliang Li,[†] Yingjie Zhou,[‡] Yaying Song,[§] Yuan Shi,[†] Wenhao Feng,[∥] Xiumei Mo,[∥] Hongyang Gao,[⊥] Qingzhu An,*[,†] and Wei Zhu*[,†]

[†]Department of Neurosurgery and [‡]Department of Hand Surgery, Huashan Hospital of Fudan University. Shanghai 200040, China

[§]Department of Neurology, Ruijin Hospital, Shanghai Jiao Tong University School of Medicine, Shanghai 200025, China

[∥]Key Laboratory of Science & Technology of Eco-Textile, Ministry of Education, College of Chemistry, Chemical Engineering and Biotechnology, Donghua University, Shanghai 201620, China

[⊥]Electron Microscopy Core Laboratory, School of Basic Medical Sciences, Fudan University, Shanghai 200433, China

S *Supporting Information*

ABSTRACT: This study explored a new rosuvastatin calcium- and heparin-loaded poly(L-lactide-co-caprolactone) (PLCL) scaffold for covered stents for treating aneurysms. The mechanism of rosuvastatin-induced endothelialization via vascular endothelial growth factor (VEGF)-A elevation was further explored. Rosu50, Rosu75, Rosu100, and phosphate-buffered saline (PBS) nanofibrous scaffolds were fabricated by coaxial electrospinning and observed by electron microscopy. Anticoagulation and pro-endothelialization properties were tested. Sixteen rabbits were selected for an in vivo assay and underwent microsurgery to establish a carotid aneurysm model. The animals were treated with covered stents and followed for 4 months using digital subtraction angiography (DSA), electron microscopy, and histology. Rosuvastatin-treated human umbilical vein endothelial cell (HUVEC) viability, function, and VEGF-A modulation were further studied to elucidate the pro-endothelialization mechanism of rosuvastatin. Our study demonstrates that rosuvastatin and heparin can be incorporated into PLCL nanofibers via electrospinning. Rosu100 nanofiber scaffolds exhibited significant anticoagulation properties. The viability of HUVECs transferred to Rosu100 nanofiber scaffolds was increased significantly. In vivo, DSA revealed that the Rosu100 group had better outcomes than the PBS group. In addition, the Rosu100 stents induced more integrated endothelialization. Further study demonstrated that rosuvastatin promoted HUVEC viability and function in vitro. The effects of rosuvastatin may be attributed to an elevation in VEGF-A. We demonstrated that rosuvastatin- and heparin-loaded PLCL-covered stents show favorable anticoagulation and pro-endothelialization properties in vitro and in vivo in a rabbit aneurysm model. VEGF-A elevation played a crucial role in rosuvastatin-promoted endothelialization. This work provides an additional option for treating cerebral aneurysms with covered stents.

KEYWORDS: cerebral aneurysm, covered stent, rosuvastatin, endothelialization, VEGF-A
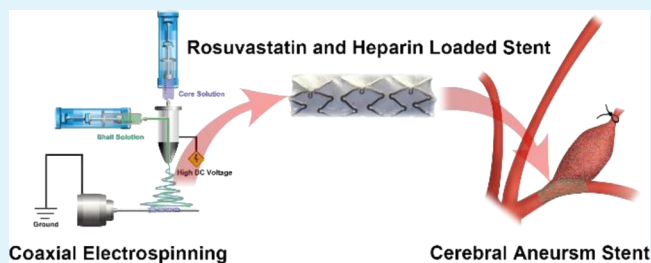
INTRODUCTION

Cerebral aneurysms are the main cause of subarachnoid hemorrhage and occur in 1−2% of patients.[1] The one-year aneurysm rupture risk is 1.4% and the five-year risk is 3.4%.[2] However, the morbidity and mortality of cerebral aneurysm growth and rupture are not ignored.

Since endovascular coiling of ruptured cerebral aneurysms was introduced in 1990,[3] endovascular aneurysm treatment options have been proven to result in better outcomes than clipping for both ruptured and unruptured aneurysms.[4] However, conventional coiling of wide-neck aneurysms is challenging. Because of the limitations in treating wide-neck aneurysms, intracranial neurovascular stents were used to treat wide-neck aneurysms in the late 1990s and early 2000s.[5−8] To avoid in-stent neointimal hyperplasia, drug-eluting stents that inhibited neointimal proliferation were applied, and stent grafts were used as mechanical barriers.[9,10] The use of covered stents increased the patency rate because of decreased restenosis after stent placement.[11]

Covered stents exclude the cerebral aneurysm dome from circulation and provide a luminal matrix for aneurysm neck endothelialization. For large vascular diseases, expanded polytetrafluoroethylene (PTFE) and polyethylene terephthalate have shown favorable properties in aneurysm exclusion
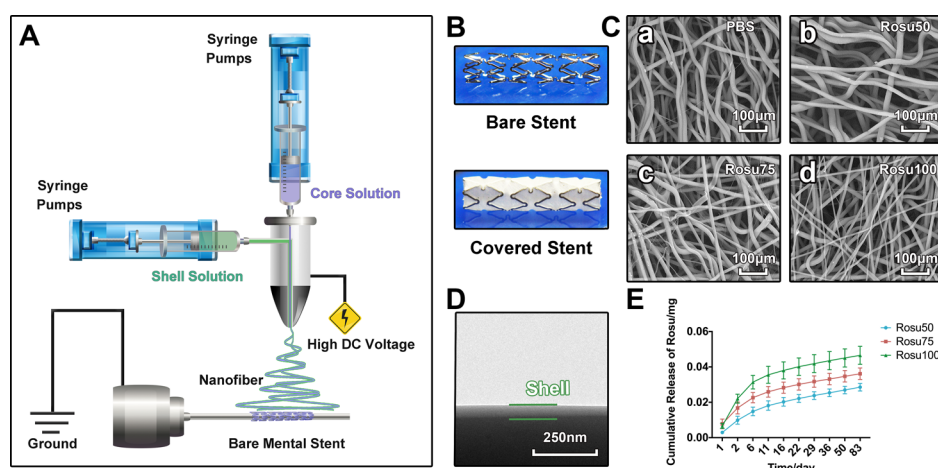
Figure 1. Characteristics of nanofiber scaffold fabrication. (A) Diagram of nanofiber scaffold-covered stent fabrication by coaxial electrospinning. (B) Photographs showing bare and covered aneurysm stents. (C) SEM images of nanofiber scaffold mats: (a) PBS, (b) Rosu50, (c) Rosu75, and (d) Rosu100. Bar = 100 μm. (D) TEM image showing the core–shell structure of the nanofibers. Bar = 250 nm. (E) Rosuvastatin release profiles from the nanofibrous mats. Data are presented as the mean $\pm$ SD; n = 3 per group.

and parent artery patency.[12–14] However, for diameters less than 6 mm, acute thrombogenesis and intimal hyperplasia are thought to be the main limitations for widespread use.[15] Saatci et al. presented an intravascular technique using coronary stent grafts to exclude aneurysms from circulation.[16] However, the coronary stent grafts were stiff and not sufficiently flexible. A Willis expanded PTFE-covered stent was designed and used for distal internal carotid artery aneurysm treatment.[17,18] To avoid intimal hyperplasia-induced in-stent restenosis and thrombosis, a novel covered stent is required.

According to our previous research, rosuvastatin shows obvious pro-endothelialization properties in aneurysm treatment.[19] In addition, we found that a heparin-loaded stent graft showed antithrombosis properties.[20] We hypothesized that heparin- and rosuvastatin-loaded covered stents would have great potential for treating aneurysms. In our previous research, we used electrospinning to fabricate rosuvastatin calcium- and heparin-loaded poly(L-lactide-co-caprolactone) (PLCL)-covered stents and tested the mechanical properties.[21] In this study, we tested the pro-endothelialization properties and underlying mechanism of the stents in vitro. Moreover, the covered stents were used in a rabbit aneurysm model with a long-term follow-up and histological observations.

METHODS

The shell solution was 120 mg/mL PLCL. The core solution was 150 mg/mL heparin and 10 mg/mL rosuvastatin. The volume ratios of heparin to rosuvastatin calcium solution were 450:50 mL, 425:75 mL, and 400:100 mL. The shell scaffold fabrication was set as PLCL, and the core solution was a different ratio of heparin and rosuvastatin. The shell solution and core solution were used to fabricate coaxial nanofibrous mats, which were designated Rosu50, Rosu75, and Rosu100. The rosuvastatin- and heparin-loaded grafts were observed and characterized by transmission electron microscopy (TEM) and scanning electron microscopy (SEM). The anticoagulation effect was tested via thromboelastography (TEG) and antithrombosis assays. Human umbilical vein endothelial cells (HUVECs) were then transferred onto the scaffolds. Live–dead cell staining and cell counting kits-8 (CCK-8) were used to assess cell viability in the scaffolds. We used SEM and phalloidin staining to evaluate cell morphology changes and attachment ability. Saccular aneurysms were created in New Zealand white rabbits as described in our previous research.[22] A covered stent was implanted under digital subtraction

angiography (DSA) guidance. All animals were followed with angiography at 4 months after covered stent implantation. The stented vascular samples were collected and used for SEM and histology. In the in vitro assay, HUVECs were treated with rosuvastatin. Changes in viability and function were evaluated by CCK-8, apoptosis, and scratch and transwell assays. The levels of vascular endothelial growth factor (VEGF)-A, VEGF-C, and VEGF-D secreted from scaffold-attached cells and rosuvastatin-treated cells were analyzed by a MILLIPLEX MAP.

Detailed methods are supplied as Supporting Information.

Statistical Analysis. SPSS (IBM) was used for statistical analysis. GraphPad prism was used for graph drawing. The coverage rate in the histological analysis, the number of cells in the transwell assay, and the apoptosis cell percentages were analyzed using independent sample t-tests. One-way ANOVA was used to assess changes in the TEG data, absorbance and viability data from the CCK-8 assay, and VEGF levels. A p value less than 0.05 was considered statistically significant.

RESULTS

Nanofiber Scaffold Fabrication and Characterization. The heparin- and rosuvastatin-loaded covered stents were prepared using coaxial electrospinning equipment (Figure 1A). A grounded rotating bare metal stent was set to collect nanofibers, thereby the bare metal stent was covered with a nanofiber scaffold (Figure 1B). Figure 1C shows SEM images of the obtained nanofiber scaffolds. The nanofibers in the scaffolds were continuous, smooth, and beadless. TEM images demonstrate the nanofiber core–shell structure. Heparin and rosuvastatin were successfully embedded in the core of the core–shell nanofibers (Figure 1D). Because the shell material shrunk under the electron beam, the nanofiber shell was relatively thin. The rosuvastatin release profiles from the nanofiber scaffolds are shown in Figure 1E. The experiments were performed in triplicate. The drug release assay showed an initial burst release over the first 6 days and a slow continuous release over the following days.

TEG and Anti-thrombosis Assay. Figure 2A shows a different state of overall coagulation that reflects both the quantity and quality of clotting factors and platelet function. Compared with the reference curve, the citrated kaolin curves of the phosphate-buffered saline (PBS) and Rosu50 groups did not show obvious anticoagulation features, whereas those of the Rosu75 and Rosu100 groups showed significant anti-
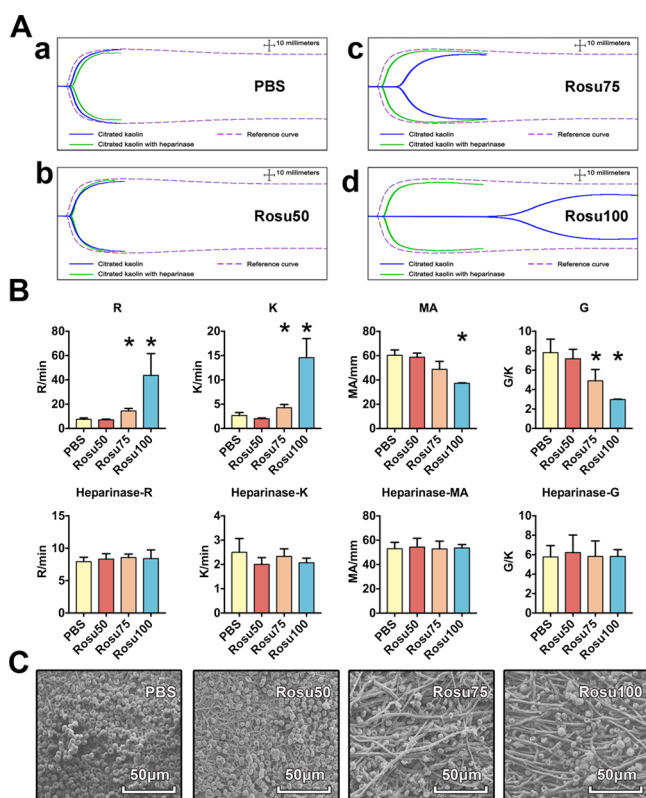
Figure 2. TEG and antithrombosis assay. (A) TEG results of the (a) PBS, (b) Rosu50, (c) Rosu75, and (d) Rosu100 groups. The dotted line shows the reference curve. The blue line shows the citrated kaolin curve. The green line shows the citrated kaolin curve with a heparanase curve. (B) Bar graphs of the clotting time (R), clot kinetics (K), and clot strength (G and MA) determined by regular TEG (upper row) and heparanase tube TEG (lower row). (C) SEM images of RBCs attached onto PBS, Rosu50, Rosu75, and Rosu100 nanofiber scaffold mats. Bar = 50 μm. Data are presented as the mean $\pm$ SD; n = 3 per group. *p < 0.05, Rosu50, Rosu75, and Rosu100 vs PBS.

coagulation. Application of heparinase cups and pins restored the curve to normal conditions in both the Rosu75 and Rosu100 groups. In the clot dynamics analysis, the R and K values were significantly elevated in the Rosu75 and Rosu100 groups compared with the PBS group. In the clot strength assay, the Rosu100 group revealed a significant decrease in the MA and G values, whereas the Rosu75 group presented a downtrend in the MA value and a significant decrease in the G value. There were no significant differences between the PBS and Rosu50 groups. In the heparanase cups and pins assay, there were no significant differences among the Rosu50, Rosu75, and Rosu100 groups (Figure 2B).

In the antithrombosis test, representative SEM images showed red blood cell (RBC) adhesion to the nanofiber scaffold mat (Figure 2C). The PBS group showed attached RBCs filling the field of view. Fewer RBCs were observed in the scaffold mat of the Rosu50 group than in that of the PBS group. The Rosu100 group, which was similar to the Rosu75 group, exhibited notable inhibition of RBC attachment.

Analysis of Attached Cell Viability and Phalloidin Staining. Confocal microscopy was used to observe propidium iodide (PI)- and calcein AM-labeled cells. No increase in the number of dead cells was observed in any of the nanofiber scaffold groups. The Rosu100 group showed more

HUVECs attached to the scaffold than the other three groups. More HUVECs were captured in both the Rosu50 and Rosu75 groups than in the PBS group, and the Rosu75 and Rosu50 groups showed similar numbers of captured HUVECs (Figure 3A). This result was also observed by SEM (Figure 3C). The
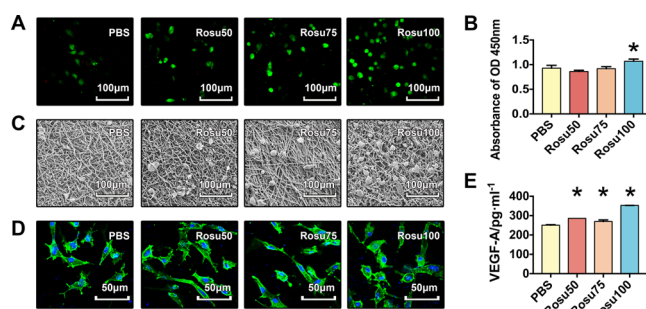
Figure 3. Viability of attached cells, cell morphology, and VEGF-A secretion. (A) Representative photographs showing viable HUVECs labeled by calcein AM and dead cells labeled by PI on the PBS, Rosu50, Rosu75, and Rosu100 nanofiber scaffold mats. Bar = 100 μm. (B) Bar graphs showing absorbance of HUVECs on the nanofiber scaffolds. (C) SEM images of HUVECs attached to the PBS, Rosu50, Rosu75, and Rosu100 nanofiber scaffold mats. Bar = 100 μm. (D) Representative photographs showing HUVECs labeled with phalloidin on the PBS, Rosu50, Rosu75, and Rosu100 nanofiber scaffold mats. Bar = 50 μm. (E) Bar graph of the levels of VEGF-A secreted by HUVECs on the nanofiber scaffolds determined via a MILLIPLEX MAP Human Angiogenesis/Growth Factor Panel. Data are presented as the mean $\pm$ SD; n = 3 per group. *p < 0.05, Rosu50, Rosu75, and Rosu100 vs PBS.

absorbance of HUVECs was recorded in each nanofiber scaffold mat with a CCK-8 kit. A significant increase in absorbance was observed in the Rosu100 group (Figure 3B).

Phalloidin staining was used to assess HUVEC morphology in the nanofiber mats. Cells were notably more extended and showed more pseudopodia in the PBS group than in the other groups. HUVECs presented a spindle-like morphology in the Rosu50 and Rosu75 groups, whereas many cells had a round and oval-shaped morphology in the Rosu100 group (Figure 3D).

Creation of a Rabbit Aneurysm Model, Stent Implantation, and Follow-Up. Saccular aneurysms were successfully established in all cases without morbidity or mortality. Figure 4A shows a schematic of aneurysm model creation and the aneurysm (arrow) during the operation. The initial schematic and angiograms before stent implantation showed direct flow into the aneurysm (arrow) of the right common carotid artery (RCCA) stump (Figure 4B). After stent implantation, the aneurysm was obliterated (Figure 4C). DSA was used for follow-up after 4 months. The follow-up angiography results were divided into types A, B, and C. Based on the DSA characteristics, therapeutic efficacy was divided into three types: type A indicated complete occlusion; type B indicated complete occlusion and small "dog ears"; and type C indicated recanalization. Six cases in the Rosu100 group and three cases in the PBS group were type A. One case in the Rosu100 group and two cases in the PBS group were type B. Three cases in the PBS group and only one case in the Rosu100 group were type C (Figure 4D).

SEM and Histology. SEM demonstrated the endothelialization level on the inner face of the implanted stent. Better endothelial coverage was found in the Rosu100 group (Figure
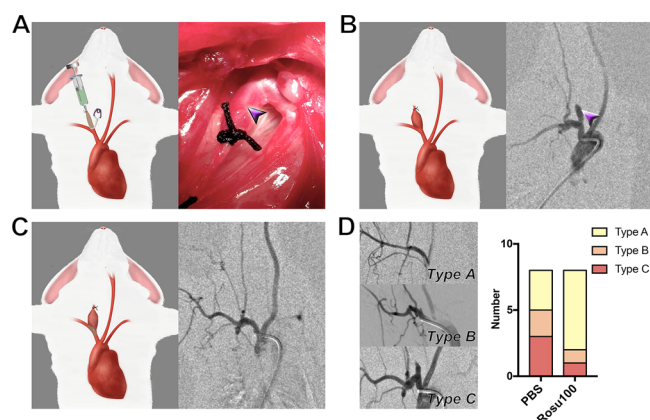
Figure 4. Creation of the rabbit aneurysm model, stent implantation, and follow-up. (A) Schematic illustration showing the creation of the rabbit aneurysm model, and a photograph showing aneurysm (arrow) formation during the operation. (B) Schematic illustration showing aneurysm formation and angiograph showing the aneurysm (arrow). (C) Schematic illustration and angiograph showing aneurysm closure after stent implantation. (D) Angiograph illustrating types A, B, and C in the long-term follow-up. Bar graph showing the number of different types in the Rosu100 group vs that in the PBS group. $n = 8$ per group.

5A(c,d)) than in the PBS group (Figure 5A(a,b)). Simple squamous epithelial cells formed a layer on the inner stent face.
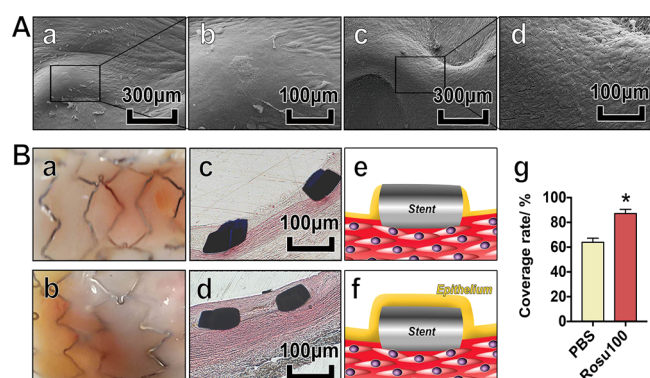
Figure 5. SEM and histology. (A) SEM images showing endothelialization of the en face of the stent. Simple squamous epithelial cells on the inner face of the stent in the PBS group (a) and Rosu100 group (c). Scale bar = 300 μm. Magnified images are shown in (b,d). Scale bar = 100 μm. (B) Image of the en face of the covered stent in the PBS group (a) and the Rosu100 group (b). Images of H&E-stained vascular sections after stent implantation in the PBS group (c) and the Rosu100 group (d). The intima coverage can be clearly observed. Bar = 100 μm. Schematic illustration showing a nonendothelialized stent (e) and an endothelialized stent (f) during the observation period. Bar graph demonstrating the coverage rate determined by H&E staining. (g) Data are presented as the mean ± SD; $n = 4$ per group. *$p < 0.05$, Rosu100 vs PBS.

Representative photos showed better intima coverage in the Rosu100 stent than in the other stents (Figure 5B(a,b)). Haematoxylin and eosin (H&E) staining demonstrated that more stent sections were covered in the Rosu100 group than in the PBS group (Figure 5B(c,d)). We quantitatively assessed the covered stent sections (Figure 5B(f,e)). Better coverage rates were shown in the Rosu100 group than in the PBS group (Figure 5B(g)).

Rosuvastatin-Treated HUVEC Viability and Function. In vitro, HUVECs were treated with rosuvastatin, and HUVEC viability was then determined by CCK-8 assay. A significant increase in absorbance was observed at 24 h using 0.01 and 0.1 μmol/L rosuvastatin, while 0.001, 0.1, 1, and 10 μmol/L rosuvastatin showed a promotional effect, and 100 μmol/L rosuvastatin showed an adverse effect at 48 h. Only 1 and 10 μmol/L rosuvastatin promoted cell viability at 72 h (Figure 6A).

To facilitate early-stage endothelialization in the functional test, 0.1 μmol/L rosuvastatin was applied for 24 h. In the apoptosis assay, the percentage of apoptotic cells was not significantly different between the control group and the rosuvastatin-treated group (Figure 6B). The transwell invasion assay demonstrated that treatment with 0.1 μmol/L rosuvastatin for 24 h increased the invasive capacity of HUVECs (Figure 6C). In the scratch assay, 24 h of 0.1 μmol/L rosuvastatin treatment greatly promoted cell migration (Figure 6D).

Analysis of VEGF-A, VEGF-C, and VEGF-D. We tested the secretion of VEGF-A, VEGF-C, and VEGF-D from HUVECs on PBS, Rosu50, Rosu75, and Rosu100 nanofiber scaffold mats. VEGF-A levels were elevated in the Rosu50, Rosu75, and Rosu100 groups compared with the PBS group. In all groups, VEGF-C levels were lower than 1.55 pg/mL, and VEGF-D levels were lower than 2 pg/mL.

The secretion of VEGF-A, VEGF-C, and VEGF-D from HUVECs after rosuvastatin treatment was also tested. At 24 h, 0.1 μmol/L rosuvastatin significantly elevated VEGF-A levels, and 1 μmol/L rosuvastatin lowered the VEGF-A level compared with those in the control group. High concentrations of rosuvastatin (10 and 100 μmol/L) reduced the level of VEGF-A at 24, 48, and 72 h, while 1, 10, and 100 μmol/L rosuvastatin reduced VEGF-C secretion at 24, 48, and 72 h, and 0.001, 0.01, and 0.1 μmol/L rosuvastatin revealed an inhibitory effect at 48 and 72 h. In the VEGF-D assessment, only 10 and 100 μmol/L rosuvastatin presented obvious decreases. However, all the values were lower than 10 pg/mL.

■ DISCUSSION

In our previous research, we evaluated nanofiber morphology, the average diameter, nanofiber inner structure, and the properties of rosuvastatin calcium- and heparin-loaded PLCL nanofiber scaffold-covered grafts.[21] In this study, the nanofiber scaffolds were used as stent coatings. We assessed the anticoagulation and pro-endothelialization properties of the different nanofiber scaffold mats. A rabbit RCCA aneurysm model was successfully established. Four months later, better endothelialization was observed in the Rosu100 group than in the PBS group via SEM and histology. In an in vitro assay, rosuvastatin promoted HUVEC growth, which may be due to an elevation in VEGF-A.

Stent implantation is often used to treat cerebral aneurysms. Saatci et al. presented an advanced reconstruction technique in which a coronary stent graft is applied in the parent artery to exclude carotid artery aneurysms from the circulation.[16] However, the coronary stent grafts used in the patients were stiff and not sufficiently flexible for use in intracranial vessels. In recent years, a flexible new stent offering a different endovascular intervention concept has been described for wide-neck or complicated aneurysms (giant, fusiform, pseudoaneurysms). Chiaradio et al. reported the use of graft stents for the treatment of fusiform aneurysms.[23] Willis
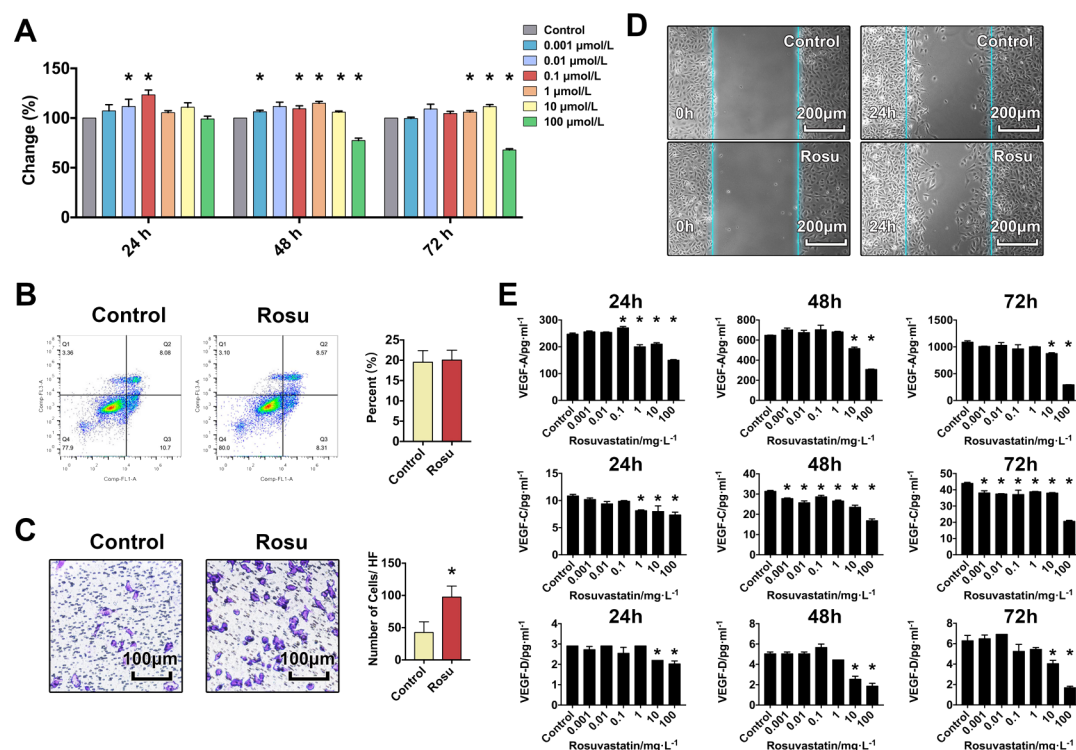
Figure 6. Rosuvastatin-treated HUVEC viability, function, and secretion of VEGF. (A) Bar graph showing the changes in HUVEC viability after 24, 48, and 72 h of rosuvastatin treatment. Data are presented as the mean ± SD; $n = 4$ per group. *$p < 0.05$. (B) Representative flow cytometry images showing HUVEC apoptosis in the control group and the 24-h rosuvastatin treatment group. Bar graph showing the percentage (%). Data are presented as the mean ± SD; $n = 3$ per group. *$p < 0.05$. (C) The migration ability of HUVECs with and without rosuvastatin treatment for 24 h as determined by the transwell assay. Representative crystal violet stained invasive cell images were shown. Scale bar = 100 μm. Bar graph showing the number of cells/HF. Data are presented as the mean ± SD; $n = 6$ per group. *$p < 0.05$. (D) Image showing HUVEC migration under control conditions (upper row) and after 24 h of rosuvastatin treatment (lower row). Scale bar = 200 μm. (E) Bar graph demonstrating the levels of VEGF-A, VEGF-C, and VEGF-D secreted by the HUVECs with and without rosuvastatin treatment as determined by a MILLIPLEX MAP Human Angiogenesis/Growth Factor Panel. Data are presented as the mean ± SD; $n = 3$ per group. *$p < 0.05$, rosuvastatin treatment vs PBS.

covered stents have also been applied to treat giant aneurysms and blister-like aneurysms.[24,25]

Electrospinning nanofiber scaffolds provide more possibilities for drug loading. Regarding pro-endothelialization, rosuvastatin, erythropoietin, and VEGF have demonstrated significant promotion effects.[19,22,26] To reduce the influence of temperature, rosuvastatin was chosen. For anticoagulation, heparin was the optimal choice according to our previous research.[20] Compared to mixture electrospinning, core−shell structures are favorable for continuous drug release. For in-stent endothelialization, local neighbor endothelial cell migration and circulating endothelial cells contribute to the endothelial layer. We assessed HUVEC attachment and cell morphology on nanofiber scaffold mats, showing that cells could stably attach to scaffold mats and that there were no shrinking cells. The stability of attached cells is important for endothelialization when the cells are exposed to blood flow. Rosuvastatin and heparin were loaded simultaneously for synergistic effects. By means of reducing the tissue factors expression and the aggregation of platelets, rosuvastatin may impair blood clot formation. As a result, both the thrombin creation and its receptor expression on the surface of the platelets are diminished. In addition to preventing clot formation, statins promote destruction of clots by decreasing plasminogen activator inhibitor-1 (PA1-1) levels and increasing fibrinolytic enzyme plasminogen expression as well.[27,28] In this study, the Rosu100 stent showed a significant advantage in both anticoagulation and HUVEC promotion in vitro. We

chose Rosu100 nanofibers for use in the animal experiment, and PBS nanofibers were used as the control. After 4 months, the Rosu100 stents showed more efficacy in aneurysm closure, and SEM and histology demonstrated more integrated endothelial layers in the Rosu100 group.

The viability and function of HUVECs after rosuvastatin treatment were analyzed in vitro, and we detected the level of VEGF in HUVECs transferred onto the rosuvastatin-loaded nanofiber scaffold mats and treated with rosuvastatin. Under rosuvastatin treatment, cell viability and function were significantly elevated. In addition, VEGF-A levels were increased. For more than a decade, the role of VEGF in the regulation of endothelialization has been under investigation. VEGF-A is the most potent pro-angiogenic protein described to date, with the ability to induce endothelial cell proliferation, vessel sprouting, and tube formation.[29] VEGF-A is also a potent survival factor for endothelial cells and has been shown to induce the expression of anti-apoptotic proteins in endothelial cells.[30,31] Although VEGF-C has been shown to be expressed in response to proinflammatory cytokines[32] and VEGF-D is known to stimulate the growth of vascular and lymphatic endothelial cells,[33] there were no obvious increases in the level of VEGF-C or VEGF-D when the HUVECs were treated with rosuvastatin in our study. Several mechanisms are engaged in the procedure of enhanced endothelial repair induced by rosuvastatin. In our study, it was found that rosuvastatin promoted endothelial cell (EC) proliferation and migration in vivo. In other words, rosuvastatin had direct

promotive effects on ECs. Besides, it was showed that statins positively act on cell survival and differentiation by inhibiting apoptotic cytokines and reducing apoptosis.[34,35] More and more, the paracrine effect of ECs may have a great contribution to the acceleration of endothelialization.[36] Further explorations are intended to reveal the mechanism of rosuvastatin in improving aneurysm stent endothelialization.

The rosuvastatin- and heparin-loaded PLCL nanofiber-covered stents used in our study were developed specifically for small-diameter vessels. The stents are sufficiently soft and flexible, and the whole body of the covered stent is radiopaque for precise placement. Additionally, the rosuvastatin- and heparin-loaded scaffolds could promote rapid endothelialization after implantation and avoid early-stage thrombogenesis. Compared with the PTFE membrane, the PLCL membrane has advantages in absorbance after stent implantation and the possibility of long-term restenosis. Additionally, PLCL nanofibers show greater potency as drug carriers. However, the strength of the PLCL membrane was inferior to that of the PTFE membrane and revealed a relatively high endoleak and recanalization rate during the follow-up period in our research.

There are still some limitations in this study. For late in-stent restenosis, the interaction between inflammation and the switch in smooth muscle cell phenotype plays an important role. This phenomenon will be assessed further over a longer follow-up period. Additionally, branch artery fate near an aneurysm limits the application of a covered stent, which requires precise stent profile selection and outstanding strength for proper adaptation to different bare stent sizes.

SUMMARY

In the present study, cerebral aneurysm stents were successfully coated with rosuvastatin- and heparin-loaded coaxial electrospun nanofiber scaffolds. In vitro studies revealed continuous rosuvastatin release from the nanofibers, with Rosu100 nanofiber scaffolds showing favorable anticoagulation and pro-endothelialization properties. The Rosu100 stent also showed a favorable therapeutic effect in a rabbit RCCA aneurysm model, as was supported by SEM and histology. We detected the mechanism of the promotion effect of rosuvastatin and found that an increase in VEGF-A plays a crucial role. Further studies are needed to explore the mechanism responsible for rosuvastatin-based endothelialization.

ASSOCIATED CONTENT

Ⓢ Supporting Information

The Supporting Information is available free of charge on the ACS Publications website at DOI: 10.1021/acsami.8b11714.

Ethics statement; scaffold fabrication by coaxial electrospinning; characterization of rosuvastatin- and heparin-loaded grafts; rosuvastatin calcium release from nanofibrous scaffolds; TEG and antithrombosis assay; live−dead cell staining; analysis of attached cell viability and phalloidin staining; creation of a rabbit aneurysm model and covered stent implantation; long-term follow-up; SEM; histology; analysis of rosuvastatin-treated HUVEC viability; apoptosis test; scratch and transwell tests; VEGF-A, VEGF-C, and VEGF-D analyses (PDF)

AUTHOR INFORMATION

Corresponding Authors

*E-mail: anqingzhu@me.com. Phone: +86-21-52887030. Fax: +86-21-62492884 (Q.A.).
*E-mail: drzhuwei@fudan.edu.cn, drweizhu@sina.com. Phone: +86-21-52887034. Fax: +86-21-62492884 (W.Z.).

ORCID Ⓘ

Xiumei Mo: 0000-0001-9238-6171
Wei Zhu: 0000-0001-7190-7476

Author Contributions

#P.L. and Y.L. contributed to this work equally.

ABBREVIATIONS

PLCL, poly(L-lactide-co-caprolactone)
TEM, transmission electron microscopy
SEM, scanning electron microscope
DSA, digital subtraction angiography
RCCA, right common carotid artery
VEGF, vascular endothelial growth factor

REFERENCES

(1) Brown, R. D., Jr.; Broderick, J. P. Unruptured Intracranial Aneurysms: Epidemiology, Natural History, Management Options, and Familial Screening. *Lancet Neurol.* **2014**, *13*, 393−404.

(2) Greving, J. P.; Wermer, M. J. H.; Brown, R. D., Jr.; Morita, A.; Juvela, S.; Yonekura, M.; Ishibashi, T.; Torner, J. C.; Nakayama, T.; Rinkel, G. J. E.; Algra, A. Development of the PHASES Score for Prediction of Risk of Rupture of Intracranial Aneurysms: A Pooled Analysis of Six Prospective Cohort Studies. *Lancet Neurol.* **2014**, *13*, 59−66.

(3) Higashida, R. T.; Halbach, V. V.; Barnwell, S. L.; Dowd, C.; Dormandy, B.; Bell, J.; Hieshima, G. B. Treatment of Intracranial Aneurysms with Preservation of the Parent Vessel: Results of Percutaneous Balloon Embolization in 84 Patients. *AJNR Am J Neuroradiol.* **1990**, *11*, 633−640.

(4) Molyneux, A. J.; Birks, J.; Clarke, A.; Sneade, M.; Kerr, R. S. C. The Durability of Endovascular Coiling Versus Neurosurgical Clipping of Ruptured Cerebral Aneurysms: 18 Year Follow-Up of the UK Cohort of the International Subarachnoid Aneurysm Trial (ISAT). *Lancet* **2015**, *385*, 691−697.

(5) Fiorella, D.; Albuquerque, F. C.; Han, P.; McDougall, C. G. Preliminary Experience Using the Neuroform Stent for the Treatment of Cerebral Aneurysms. *Neurosurgery* **2004**, *54*, 6−17.

(6) Henkes, H.; Bose, A.; Felber, S.; Miloslavski, E.; Berg-Dammer, E.; Kühne, D. Endovascular Coil Occlusion of Intracranial Aneurysms Assisted by a Novel Self-Expandable Nitinol Microstent (Neuroform). *Interv. Neuroradiol.* **2002**, *8*, 107−119.

(7) Higashida, R. T.; Smith, W.; Gress, D.; Urwin, R.; Dowd, C. F.; Balousek, P. A.; Halbach, V. V. Intravascular stent and endovascular coil placement for a ruptured fusiform aneurysm of the basilar artery. *J. Neurosurg.* **1997**, *87*, 944−949.

(8) Mericle, R. A.; Lanzino, G.; Wakhloo, A. K.; Guterman, L. R.; Hopkins, L. N. Stenting and Secondary Coiling of Intracranial Internal Carotid Artery Aneurysm: Technical Case Report. *Neurosurgery* **1998**, *43*, 1229−1233.

(9) Serruys, P. W.; Kutryk, M. J. B.; Ong, A. T. L. Coronary-Artery Stents. *N. Engl. J. Med.* **2006**, *354*, 483−495.

(10) Katsanos, K.; Karnabatidis, D.; Kitrou, P.; Spiliopoulos, S.; Christeas, N.; Siablis, D. Paclitaxel-Coated Balloon Angioplasty vs. Plain Balloon Dilation for the Treatment of Failing Dialysis Access:6-Month Interim Results From a Prospective Randomized Controlled Trial. *J. Endovasc. Ther.* **2012**, *19*, 263−272.

(11) Hajibandeh, S.; Hajibandeh, S.; Antoniou, S. A.; Torella, F.; Antoniou, G. A. Covered vs Uncovered Stents for Aortoiliac and Femoropopliteal Arterial Disease. *J. Endovasc. Ther.* **2016**, *23*, 442−452.

(12) Pavani, M.; Cerrato, E.; Latib, A.; Ryan, N.; Calcagno, S.; Rolfo, C.; Ugo, F.; Ielasi, A.; Escaned, J.; Tespili, M.; Conrotto, F.; Mancone, M.; Colombo, A.; Varbella, F. Acute and long-term outcomes after polytetrafluoroethylene or pericardium covered stenting for grade 3 coronary artery perforations: Insights from G3-CAP registry. *Catheter Cardiovasc Interv* **2018**, DOI: 10.1002/ccd.27789.

(13) Takano, M.; Yamamoto, M.; Inami, S.; Xie, Y.; Murakami, D.; Okamatsu, K.; Ohba, T.; Seino, Y.; Mizuno, K. Delayed Endothelialization After Polytetrafluoroethylene-Covered Stent Implantation for Coronary Aneurysm. *Circ. J.* **2009**, *73*, 190−193.

(14) Namba, Y.; Yamanaka, T.; Ida, J.; Oka, T. Implantation of Multiple Polytetrafluoroethylene Covered Stent Inside Drug Eluting Stent to Rescue Purulent Coronary Artery Ectasia with Giant Saccular Aneurysm. *Int. J. Cardiovasc. Imaging* **2018**, *34*, 1143−1146.

(15) Desai, M.; Seifalian, A. M.; Hamilton, G. Role of Prosthetic Conduits in Coronary Artery Bypass Grafting. *Eur. J. Cardiothorac. Surg.* **2011**, *40*, 394−398.

(16) Saatci, I.; Cekirge, H. S.; Ozturk, M. H.; Arat, A.; Ergungor, F.; Sekerci, Z.; Senveli, E.; Er, U.; Turkoglu, S.; Ozcan, O. E.; Ozgen, T. Treatment of Internal Carotid Artery Aneurysms with a Covered Stent: Experience in 24 Patients with Mid-Term Follow-Up Results. *AJNR Am J Neuroradiol.* **2004**, *25*, 1742−1749.

(17) Li, M.-H.; Li, Y.-D.; Tan, H.-Q.; Luo, Q.-Y.; Cheng, Y.-S. Treatment of Distal Internal Carotid Artery Aneurysm with the Willis Covered Stent: A Prospective Pilot Study. *Radiology* **2009**, *253*, 470−477.

(18) Li, M.-H.; Li, Y.-D.; Gao, B.-L.; Fang, C.; Luo, Q.-Y.; Cheng, Y.-S.; Xie, Z.-Y.; Wang, Y.-L.; Zhao, J.-G.; Li, Y.; Wang, W.; Zhang, B.-L.; Li, M. A New Covered Stent Designed for Intracranial Vasculature: Application in the Management of Pseudoaneurysms of the Cranial Internal Carotid Artery. *AJNR Am J Neuroradiol.* **2007**, *28*, 1579−1585.

(19) Liu, P.; An, Q.; Chen, X.; Huang, J.; Yang, G.-Y.; Zhu, W. Rosuvastatin for Enhancement of Aneurysm Neck Endothelialization After Coil Embolization: Promotion of Endothelial Progenitor Cells in a Rodent Model. *J. Neurosurg.* **2016**, *124*, 1265−1274.

(20) Wang, J.; An, Q.; Li, D.; Wu, T.; Chen, W.; Sun, B.; Ei-Hamshary, H.; Al-Deyab, S. S.; Zhu, W.; Mo, X. Heparin and Vascular Endothelial Growth Factor Loaded Poly(L-Lactide-Co-Caprolactone) Nanofiber Covered Stent-Graft for Aneurysm Treatment. *J. Biomed. Nanotechnol.* **2015**, *11*, 1947−1960.

(21) Feng, W.; Liu, P.; Yin, H.; Gu, Z.; Wu, Y.; Zhu, W.; Liu, Y.; Zheng, H.; Mo, X. Heparin and Rosuvastatin Calcium-Loaded Poly(L-Lactide-Co-Caprolactone) Nanofiber-Covered Stent-Grafts for Aneurysm Treatment. *New J. Chem.* **2017**, *41*, 9014−9023.

(22) Chen, X.; Wang, J.; An, Q.; Li, D.; Liu, P.; Zhu, W.; Mo, X. Electrospun poly(l-lactic acid-co-ε-caprolactone) fibers loaded with heparin and vascular endothelial growth factor to improve blood compatibility and endothelial progenitor cell proliferation. *Colloids Surf., B* **2015**, *128*, 106−114.

(23) Chiaradio, J. C.; Guzman, L.; Padilla, L.; Chiaradio, M. P. Intravascular Graft Stent Treatment of a Ruptured Fusiform Dissecting Aneurysm of the Intracranial Vertebral Artery: Technical Case Report. *Neurosurgery* **2002**, *50*, 213−217.

(24) Wang, J. B.; Li, M. H.; Fang, C.; Wang, W.; Cheng, Y. S.; Zhang, P. L.; Du, Z. Y.; Wang, J. Endovascular Treatment of Giant Intracranial Aneurysms with Willis Covered Stents. *Neurosurgery* **2008**, *62*, E1176−E1177.

(25) Zhang, Y.; Zhang, Y.; Liang, F.; Jiang, C. Procedure-Related Complication of Willis Covered Stent in the Treatment of Blood Blister-Like Aneurysm: Stent Detachment from Dilating Balloon. *Front. Neurol.* **2017**, *8*, 639.

(26) Liu, P.; Zhou, Y.; An, Q.; Song, Y.; Chen, X.; Yang, G.-Y.; Zhu, W. Erythropoietin Stimulates Endothelial Progenitor Cells to Induce Endothelialization in an Aneurysm Neck After Coil Embolization by Modulating Vascular Endothelial Growth Factor. *Stem Cells Transl. Med.* **2016**, *5*, 1182−1189.

(27) Sahebkar, A.; Catena, C.; Ray, K.; Vallejo-Vaz, A.; Reiner, Ž.; Sechi, L.; Colussi, G. Impact of statin therapy on plasma levels of plasminogen activator inhibitor-1. *Thromb. Haemostasis* **2016**, *116*, 162−171.

(28) Stanley, F. M.; Linder, K. M.; Cardozo, T. J. Statins Increase Plasminogen Activator Inhibitor Type 1 Gene Transcription Through a Pregnane X Receptor Regulated Element. *PLoS One* **2015**, *10*, No. e0138097.

(29) Ferrara, N.; Gerber, H.-P.; LeCouter, J. The Biology of VEGF and Its Receptors. *Nat. Med.* **2003**, *9*, 669−676.

(30) Gerber, H.-P.; Dixit, V.; Ferrara, N. Vascular Endothelial Growth Factor Induces Expression of the Antiapoptotic Proteins Bcl-2 and A1 in Vascular Endothelial Cells. *J. Biol. Chem.* **1998**, *273*, 13313−13316.

(31) Benjamin, L. E.; Keshet, E. Conditional Switching of Vascular Endothelial Growth Factor (VEGF) Expression in Tumors: Induction of Endothelial Cell Shedding and Regression of Hemangioblastoma-Like Vessels by VEGF Withdrawal. *Proc. Natl. Acad. Sci. U. S. A.* **1997**, *94*, 8761−8766.

(32) Ristimäki, A.; Narko, K.; Enholm, B.; Joukov, V.; Alitalo, K. Proinflammatory Cytokines Regulate Expression of the Lymphatic Endothelial Mitogen Vascular Endothelial Growth Factor-C. *J. Biol. Chem.* **1998**, *273*, 8413−8418.

(33) Akahane, M.; Akahane, T.; Matheny, S. L.; Shah, A.; Okajima, E.; Thorgeirsson, U. P. Vascular Endothelial Growth Factor-D is a Survival Factor for Human Breast Carcinoma Cells. *Int. J. Cancer* **2005**, *118*, 841−849.

(34) Henrich, D.; Seebach, C.; Wilhelm, K.; Marzi, I. High Dosage of Simvastatin Reduces TNF-α-Induced Apoptosis of Endothelial Progenitor Cells but Fails to Prevent Apoptosis Induced by IL-1β In Vitro. *J. Surg. Res.* **2007**, *142*, 13−19.

(35) Zaitone, S. A.; Abo-Gresha, N. M. Rosuvastatin Promotes Angiogenesis and Reverses Isoproterenol-Induced Acute Myocardial Infarction in Rats: Role of Inos and VEGF. *Eur. J. Pharmacol.* **2012**, *691*, 134−142.

(36) He, T.; Smith, L. A.; Harrington, S.; Nath, K. A.; Caplice, N. M.; Katusic, Z. S. Transplantation of Circulating Endothelial Progenitor Cells Restores Endothelial Function of Denuded Rabbit Carotid Arteries. *Stroke* **2004**, *35*, 2378−2384.